# Multiprobe analyses on nucleation and evolution of nanocrystallization process in a high saturation magnetization soft magnetic Fe-Si-B-P-Cu-C alloy

Shozo Hiramoto[1,2]*, Satoshi Okamoto[2,3], Jun Uzuhashi[3], Tadakatsu Ohkubo[3], Akihiko Toda[1], Sangwook Kim[1], Chikako Moriyoshi[1] and Yoshihiro Kuroiwa[1]

[1] Graduate School of Advanced Science and Engineering, Hiroshima University, Higashihiroshima739-8527 Japan

[2] Institute of Multidisciplinary Research for Advanced Materials, Tohoku University, Sendai 980-0812 Japan

[3] National Institute for Materials Science, Tsukuba 305-0047 Japan

## ABSTRACT

This study aimed to explore the impact of annealing temperature on the nucleation and subsequent growth of nanocrystalline α-Fe grains in a high saturation magnetization soft magnetic $Fe_{84.8}Si_{0.5}B_{9.4}P_{3.5}Cu_{0.8}C_{1.0}$ alloy. Thus, we conducted multiprobe analyses of the isothermal crystallization process within 633–733 K. Transmission electron microscopy and atom probe tomography observations of the samples isothermally annealed at 733 and 633 K revealed distinct differences in their microstructures. In case of the higher isothermal temperature, larger Cu clusters were observed, whereas the α-Fe grains were finer. In contrast, in case of the lower isothermal temperature, the Cu clusters were smaller, and the α-Fe grains were coarser. Time-resolved synchrotron radiation X-ray diffraction measurements confirmed the sporadic nucleation mechanism, highlighting the significant effect of isothermal temperature on the formation of α-Fe grains. To achieve an optimal microstructure for lower coercivity, the Cu clustering and α-Fe nanocrystallization must be controlled by annealing at higher temperatures for shorter durations.

Keywords: Soft magnetic materials, nanocrystallization, microstructure, *in situ* synchrotron radiation X-ray diffraction

## Introduction

The effective use of limited energy resources is required for the development of a sustainable society. Soft magnetic materials are used in various energy-conversion devices; therefore, advances in the improved functionalities and optimized manufacturing processes of these materials exert a significant impact on society[1]. To facilitate the application of energy conversion devices such as motor cores and transformers, materials with high saturation magnetization $M_s$ and low coercivity $H_c$ are crucial for downsizing devices while maintaining low energy losses. Nanocrystalline materials are among the best candidates for this requirement owing to their unique microstructure comprising uniformly dispersed nanocrystalline α-Fe grains in an amorphous matrix phase. If ideal nanocrystalline materials can be put to practical use, motors and transformers will become smaller, and power loss will be greatly reduced. In nanocrystalline soft magnetic materials, the relationship between the coercivity and grain

size can be explained by the random magnetic anisotropy model [2]. Intergrain exchange coupling reduces the effective magnetic anisotropy with respect to the square root of the number of grains involved in the exchange length, resulting in excellent soft magnetic properties. The Fe–Si–B–Nb–Cu alloy [3] was the first to be developed and remains the most popular nanocrystalline soft magnetic material. Therefore, the microstructure and nanocrystallization mechanisms of this alloy have been extensively investigated. Cu clusters are formed during the early stages of crystallization to initiate the nucleation of α–Fe(–Si) grains while Nb functions as an inhibitor for Fe–Si grain coarsening [4, 5]. Thus, the grain growth of nanocrystalline α-Fe(–Si) grains is understood as the diffusion-controlled reactions [6, 7] rather than the phase boundary-controlled kinetics. Despite the excellent soft magnetic properties and well established nanocrystallization processes of Fe–Si–B–Nb–Cu alloy, its $M_s$ (approximately 1.2 T) is not sufficient for the above recent demands.

During the past 15 years, novel nanocrystalline soft magnetic alloys such as Fe–Si–B–Cu [8], Fe–Si–B–P–Cu(–C) [9], Fe–B–P–Cu [10], and Fe–B[11] have been developed. They have garnered attention owing to their high $M_s$ of 1.7–1.9 T achieved by increasing the Fe content and removing the heavy element of Nb. However, a nanocrystalline structure with excellent soft magnetic properties requires rapid thermal annealing [5, 11-14], which is disadvantageous for commercial use. Among them, P in Fe–Si–B–P–Cu(–C) alloy functions as an inhibitor for α–Fe grain coarsening although its effect is weaker than that of Nb in Fe–Si–B–Nb–Cu [15]. Therefore, the well-composition-designed Fe–Si–B–P–Cu(–C) alloy has the potential for practical applications. Increasing the P content mitigates the heating rate sensitivity of nanocrystallization [16, 17]. However, the addition of large amounts of P lowers the Fe content and results in a lower *Ms* [10]. Moreover, small amounts of C and Si are effective, as C lowers the melting point of precursor amorphous phase and stabilizes the casting process [18], while Si facilitates the formation of the nanocrystalline structure as it expands the temperature gap between the crystallization onsets of α-Fe and other compounds [19]. However, the annealing conditions for this alloy are complex, and there are difficulties in optimizing the industrial process.

However, the nanocrystallization mechanism of Fe–Si–B–P–Cu(–C) alloys remains unclear. Few studies have reported the different nanocrystallization processes of this alloy compared with those of Fe–Si–B–Nb–Cu alloys. In these studies, the local structure of Cu clusters changed from face-centered cubic (fcc) to body-centered cubic (bcc) in the early stages of crystallization [20] and a mode change of crystallization was found with increasing annealing temperature in Fe–Si–B–P–Cu(–C) alloys at a relatively slow heating rate of 6.7 $Ks^{-1}$ [21]. Because the soft magnetic properties in Fe–Si–B–P–Cu(–C) alloys are governed by their nanocrystalline microstructure, the development of the nanocrystalline microstructure during the annealing process must be understood.

This study performed multiprobe analyses using transmission electron microscopy (TEM), atom probe tomography (APT), and *in situ* time-resolved synchrotron radiation X-ray diffraction (SRXD) and discussed the nanocrystalline mechanism of an Fe-Si-B-P-Cu-C alloy. In particular, *in situ* SRXD is a powerful method for investigating the crystallization kinetics of Fe–Si–B–P–Cu–C alloys under an isothermal process. It provides significant insights into the nanocrystallization mechanism and

guidelines for the temperature control of soft magnetic materials in industrial applications.

**Experimental Procedure**

The alloy used in this study was $Fe_{84.8}Si_{0.5}B_{9.4}P_{3.5}Cu_{0.8}C_{1.0}$. Pure iron, silicon, iron boron, iron phosphorus, copper, and carbon were used as the raw materials. First, the master alloy was prepared via arc melting in an Ar atmosphere. Precursor amorphous ribbons were produced using a single-roller melt-spinning method. The master alloy was melted in a high-frequency melting furnace and quenched continuously on the Cu-roll. Consequently, 50 mm wide and 25 μm thick precursor amorphous alloy ribbons were casted. *In situ* SRXD was performed using a SPring-8 BL02B2 [22]. To obtain the diffraction intensities of the transmission geometry, the amorphous alloy precursor was inserted into a quartz capillary with a 0.3 mm in diameter. The capillary interior was filled with Ar gas and sealed to prevent oxidation. A synchrotron radiation X-ray energy of 25 keV was selected, and the diffraction intensities were measured using a two-dimensional flat-panel detector. The wavelength was obtained as 0.04962 nm via calibration with $CeO_2$ powder. The isothermal process was performed using a nitrogen gas blowing device. The isothermal temperature was 633–733 K. In this temperature range, crystallization of α-Fe occurred and no other crystalline compounds were formed [23]. The accuracy of temperature measurements was confirmed using K-type thermocouples. The heating rate was 400 $Ks^{-1}$ in this experimental configuration. This is an ideal high heating rate that facilitates the isothermal experiments. X-ray diffraction profiles were acquired every 1 s. Therefore, a continuous change in the diffraction profile owing to nanocrystallization during the isothermal process was observed. We carefully observed the changes in the diffraction patterns for each temperature and took sufficient annealing time until the crystallization process was completed. The grain size was calculated using the Scherrer equation [24]. The grain size was calibrated using the width at half maximum of the diffraction intensity of a standard sample of $LaB_6$ powder as the instrumental function. The application of the Scherrer equation is discussed in the Supplementary Material (Online Resource 1). The crystallinity was approximately evaluated from the ratio of the integrated intensity of the (110) peak of α-Fe to the broad intensity derived from the amorphous [25]. To characterize the magnetic properties of the samples, the coercivity $H_c$ was measured using a DC B-H loop tracer (Riken Denshi, BHS-40) with a maximum field of 2 $kAm^{-1}$. The microstructures of the samples isothermally annealed at 633 and 733 K for 100 and 20 min, respectively, were observed using TEM (FEI Titan G2 80-200) and APT (CAMECA LEAP5000 XS). TEM samples were fabricated using a standard lift-out method, and these for APT samples were prepared by the automated tip preparation script [26, 27] using focused ion beam milling. The thickness of the TEM samples is approximately 50-60 nm, and the tip radius of curvature and its shank angle for APT analysis is controlled to 50 nm and 25 degrees. APT observations were performed in the 355 nm wavelength laser pulsing mode at a repetition rate of 500 kHz with a laser pulse energy of 50 pJ at a base temperature of 30 K. The detection rate was kept constant at 2.0%, that is, the detection of one ion per 50 laser pulses. The obtained APT data were analyzed using CAMECA IVAS 6.3 software.

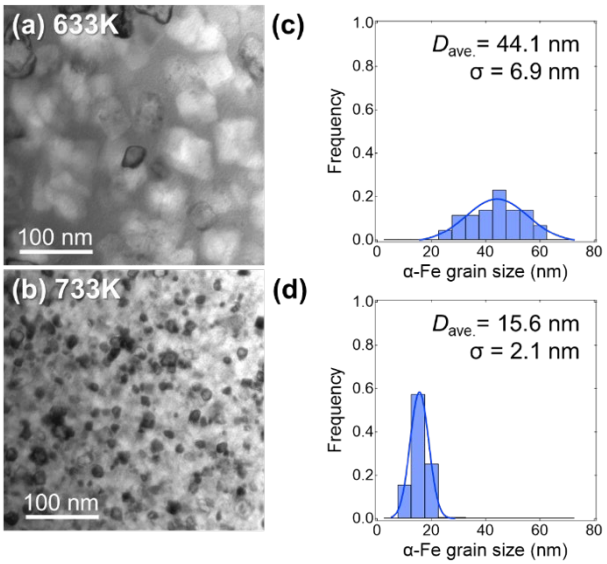


Figure. 1 BF–TEM images of the samples isothermally annealed at (a) 633 and (b) 733 K, respectively. α-Fe grain size distributions of the samples at (c) 633 and (d) 733 K, respectively. Averaged α-Fe grain size $D_{ave.}$ is 44.1 and 15.6 nm for 633 and 733 K, respectively. The curves in (c) and (d) are the result of fitting with a Gaussian function.

## Results and discussion

### TEM and APT observations

Figures 1(a) and 1(b) show the Bright-Field TEM (BF–TEM) images of the microstructure comprising α-Fe and residual amorphous phases in the samples isothermally annealed at 633 and 733 K, respectively. Figures 1(c) and 1(d) show the α-Fe grain size distributions and averaged α-Fe grain size $D_{ave.}$, respectively, evaluated from the BF-TEM images. The α-Fe gain size was finer for the higher annealing temperature than that for the lower annealing temperature. The lower temperature annealing coarsened the α-Fe grains. A comparison of the values of standard deviation $\sigma$ evaluated from the Gaussian fitting for the grain size distribution revealed that the distribution became narrower for high temperature isothermal annealing than that for low temperature annealing. Details of the particle analysis and additional BF-TEM images, including intermediate temperatures, are described in the Supplementary Materials (Online Resources 2). Thus, isothermal annealing at high temperature caused a uniformly distributed nanocrystalline α-Fe grains rather than the low temperature annealing. Figure 2 shows the APT images of the two samples annealed at 633 and 733 K. Figures 2(a) and 2(b) show the 3-dimensional (3D) distribution maps of the Fe concentration. Figures 2(c) and 2(d) show the typical 2 nm-sliced maps for B, P, and Cu atoms. The red areas in Figs. 2(a) and 2(b) are high-Fe-concentration regions, and their sizes are consistent with the BF–TEM results (Fig. 1). The enrichment of P atoms at the boundaries between the Fe grains and the residual amorphous phase was clearly observed in Figs. 2(c) and 2(d), as observed in the previous literature [17]. However, the distributions and sizes of the Cu clusters in Figs. 2(c) and 2(d) were quite different. At lower annealing temperatures,

the Cu clusters were densely distributed with a smaller size than those at higher annealing temperatures.

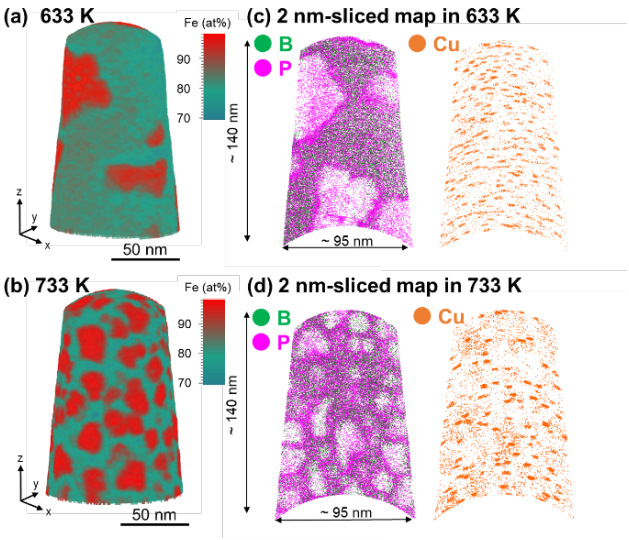


Figure. 2 3D distribution maps of Fe atoms obtained by APT for the annealing temperature of (a) 633 and (b) 733 K, respectively. Two nm sliced distribution images of B, P. and Cu atoms for the annealing temperature of (c) 633 and (d) 733 K, respectively.

Table 1 summarizes the results of the statistical analyses of the APT and TEM observations for the samples annealed at 633 and 733 K, respectively. The density of α-Fe grains was approximately two times higher at 733 K than that at 633 K. In this analysis, crystallinity was defined as the volume ratio of the region with more than 85 at.% of Fe. The crystallinities at 633 and 733 K were evaluated to be 42% and 56%, respectively. The average sizes of the Cu cluster were 3.6 and 2.5 nm at 733 K and 633 K, respectively. In contrast, the density of Cu clusters was higher at 633 K than that at 733 K. These results suggest that larger Cu clusters are effective in forming α-Fe grains with uniform and fine sizes. Similar results were reported for the samples with different compositions by Nomura *et al.*[17]. Therefore, these findings would be a universal feature related to the size of Cu clusters and the nanocrystallization of α-Fe grains.

Table 1. Results of statistical analyses of APT/TEM images for the isothermal annealing at 633 and 733 K.

| | | 633 K | 733 K |
|---|---|---|---|
| α-Fe grains from TEM/APT | Number density | $0.7 \times 10^{22}$ m$^{-3}$ | $13.4 \times 10^{22}$ m$^{-3}$ |
| | Average size | 44.1 nm | 15.6 nm |
| | Volume Fraction | 42% | 56% |
| Cu clusters from APT | Number density | $2.6 \times 10^{24}$ m$^{-3}$ | $1.8 \times 10^{24}$ m$^{-3}$ |
| | Average size | 2.5 nm | 3.6 nm |
| | Average number of Cu clusters | 45.5 atoms /cluster | 124.7 atoms/ cluster |

### *in situ* SXRD

To investigate these behaviors, *in situ* time-resolved SXRD was performed under isothermal conditions as shown in Fig. 3. In the SRXD profiles, the diffraction peaks from Cu clusters could not be obtained even using an extremely high brilliant synchrotron radiation X-ray beam. This may be owing to the very small Cu content of 1 at. % and their very small cluster size of 2–3 nm. The representative elapsed time dependences of the α–Fe (110) diffraction profiles at 633, 673, and 733 K are shown in Figs. 3(a), 3(b), and 3(c), respectively. Figure 3(d) shows the intensity maps of these α–Fe (110) diffractions for 633–733 K. From these time evolutions of α–Fe (110) diffraction, the time dependence of grain size α–Fe and crystallinity were evaluated, as shown in Figs. 3(e) and (f), respectively. As evident, the well-evolved grain size of α–Fe strongly depended on the isothermal temperature, that is, the grain size α–Fe decreased with increasing temperature. Moreover, the well-evolved grain sizes of α-Fe for the temperatures of 733 and 633 K are quantitatively consistent with those observed in BF-TEM and APT, as shown in Table 1. Therefore, the isothermal *in situ* SRXD experiments well reproduced the annealing process of the Fe–Si–B–P–Cu–C alloy. The evolution time of the α–Fe grain size also strongly depended on the temperature. The evolution time at a temperature of 633 K was approximately 100 min, and it shortened at higher temperatures. Finally, the evolution time for the temperature of 733 K was shorter than the first time step of the *in situ* SRXD experiment. Thus, the crystallization of α–Fe grains at 733 K was completed in less than a few seconds. Similar to the behavior of grain size, the crystallinity strongly depended on the isothermal temperature. A higher crystallinity with a shorter evolution time was obtained at a higher isothermal temperature. Therefore, the smaller α–Fe grains with high density evolved faster for the higher isothermal temperature and vice versa.

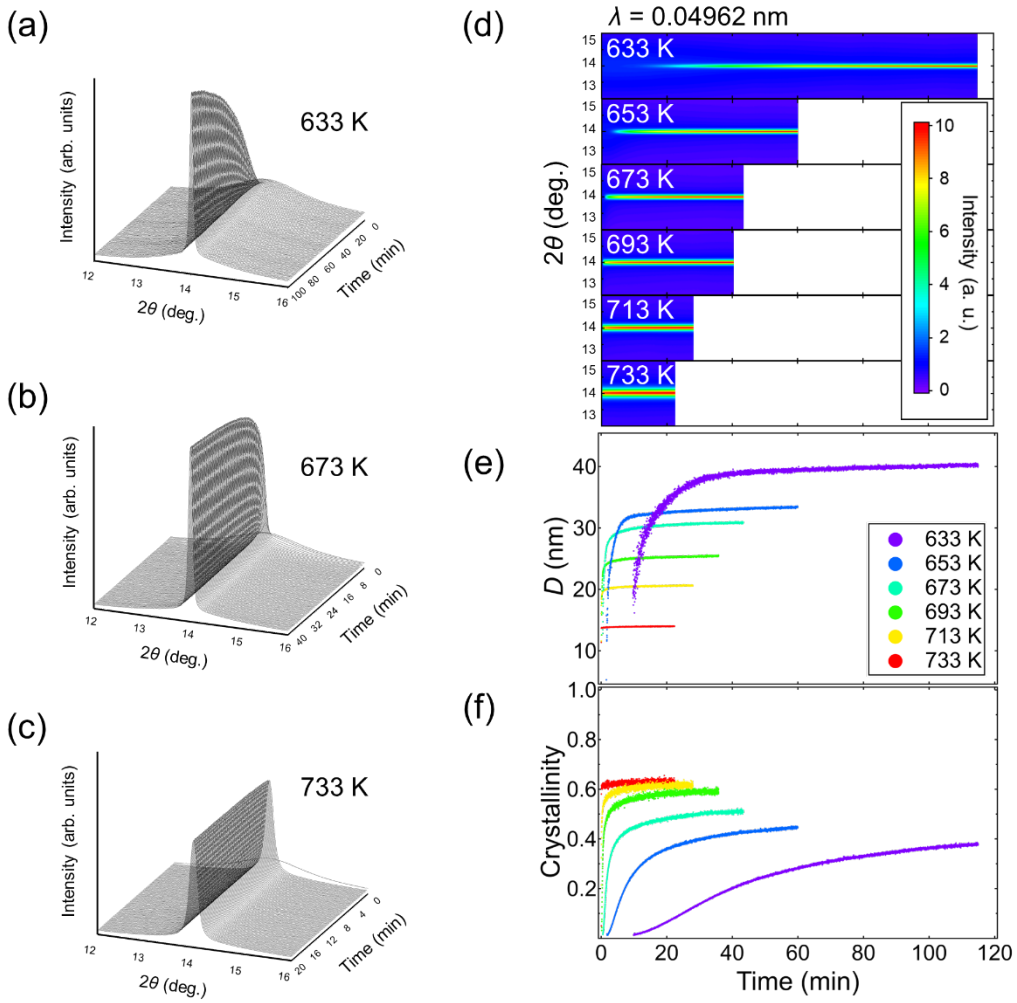


Figure. 3 Elapsed time dependences of α-Fe (110) diffraction profiles at the isothermal temperature of (a)633, (b)673, and (c)733 K, respectively. (d) Intensity maps of α–Fe (110) diffractions, (e) grain size *D*, and (f) crystallinity, respectively, as a function of elapsed time for the isothermal temperature range of 633–733 K.

Table 2 summarizes the *in situ* SXRD data of the isothermal elapsed time, grain size *D,* and crystallinity for each temperature of the isothermal process. The coercivity $H_c$ is also presented in this table. As evident, the high-temperature isothermal process resulted in a fine grain size and low $H_c$.

Table 2. SXRD data of elapsed time, grain size *D*, crystallinity, and coercivity $H_c$ for various temperatures of isothermal process

| $T_a$ (K) | Time (min) | *D* (nm) | Crystallinity | $H_c$ (A/m) |
|---|---|---|---|---|
| 633 | 100 | 40.1 | 37.6% | 98.0 |
| 653 | 60 | 33.4 | 44.8% | 47.9 |
| 673 | 40 | 30.9 | 50.7% | 18.6 |

| | | | | |
|---|---|---|---|---|
| 693 | 40 | 25.5 | 60.1% | 11.4 |
| 713 | 20 | 20.6 | 61.3% | 7.5 |
| 733 | 20 | 14.0 | 63.7% | 6.1 |

The Avrami model (Kolmogorov–Johnson–Mehl–Avrami model) [28-32] was applied to analyze the kinetics of the nanocrystallization process, and the nucleation and subsequent grain growth mechanisms were discussed. Under the isothermal conditions, Eq. (1) of the Avrami model describes the time evolution of the volume fraction $\varphi$ of the transformation in the alloy, that is, the relative crystallinity normalized with the well-evolved crystallinity.

$$\varphi = 1\text{-}\exp\{-k(t-\tau)^n\} \quad (1)$$

where $n$ is the Avrami exponent, $k$ is a constant, $t$ is the elapsed time, and $\tau$ is the incubation time, which is the time lag to begin the crystallization.

If the grain size $D$ is proportional to the power law of the elapsed time, the growth mechanism of the nanocrystalline grains can be discussed thermodynamically using Eq. (2) [33, 34].

$$D = A(t-\tau)^{\beta} \quad (2)$$

where $A$ is a constant. For example, when $D \propto (t-\tau)^{1/2}$ is obtained, it can be explained as the growth mechanism under the diffusion-controlled reactions[35]. The relationship between $n$ in Eq. (1) and $\beta$ in Eq. (2) is expressed as: n = 3$\beta$ for instantaneous nucleation from foreign heterogeneities; and $n$ = 1+3$\beta$ for sporadic nucleation from homogeneous media or foreign heterogeneities.

Table 3 presents the *in situ* SXRD analysis results of the $n$, $\beta$, and 1 + 3$\beta$. For the temperature range of 633–713 K, the experimentally determined values of $n$ and $\beta$ were closer to the relation of $n$ = 1+3$\beta$ rather than $n$ = 3$\beta$. Thus, the nucleation mechanism of nanocrystalline α–Fe grains was explainable by the sporadic nucleation process. Comparisons of the time dependences of grain size of α–Fe and crystallinity in Figs. 3(e) and 3(f) revealed that the crystallinity gradually continued to increase after the grain size appeared to be almost saturated. These behaviors would support the sporadic nucleation process, Regretfully, the analysis based on the Avrami model was not applicable for the temperature of 733 K owing to the lack of experimental data in the short time region. However, according to the temperature dependences of $n$ and $\beta$ in Table 3, the sporadic nucleation process appears to be independent of the temperature of isothermal process. Here, the values of $\beta$ were smaller than 1/2, implying that the grain growth of α-Fe was delayed rather than that expected from the usual diffusion-controlled reactions. This delay in α–Fe grain growth may be owing to the strain induced at the boundary of the α–Fe grain and residual amorphous phase [36].

Table 3. Results of Avrami exponent $n$, $\beta$, and $1+3\beta$,

| $T_a$ (K) | $n$ | $\beta$ | $1+3\beta$ |
|---|---|---|---|
| 633 | 1.36 | 0.25 | 1.75 |
| 653 | 1.30 | 0.22 | 1.66 |
| 673 | 1.40 | 0.15 | 1.45 |
| 693 | 1.10 | 0.07 | 1.21 |
| 713 | 0.79 | 0.05 | 1.15 |
| 733 | NA | NA | NA |

The relationship between the size of Cu clusters obtained by the APT observations and the kinetics of α-Fe grains obtained by *in situ* SXRD is discussed. The nucleation of α-Fe grains occurred sporadically and followed the diffusion-controlled reactions. These nucleation behaviors were insensitive to the isothermal annealing temperature. However, the uniformity of microstructure, α-Fe grain size, crystallinity, and Cu cluster size strongly depended on the isothermal annealing temperature. For higher temperature, the Cu clusters were larger than 3 nm, and the microstructure of well-distributed smaller α–Fe grain with higher crystallinity was obtained. However, for lower temperature, the Cu clusters were smaller than 3 nm, and larger α-Fe grains were less distributed with lower crystallinity. Cu clusters are known to precipitate before the nanocrystallization of α–Fe in the precursor amorphous alloys [37-41]. Therefore, it is highly possible that the larger Cu clusters function as the nucleation sites for α-Fe grain. The nucleation of α-Fe took place sporadically but proceeded at a very high rate, resulting in the well distributed smaller α-Fe grains. Whereas, the smaller Cu clusters did not work as the nucleation sites for α-Fe grains. Consequently, the sporadic nucleation of α-Fe grains proceeded slowly, resulting in the coarsening α-Fe grain with less distributed. Conventional kinetic studies of soft magnetic nanocrystalline materials have mostly been based on DSC-based calorimetric analysis[21, 42], with recent studies of kinetic using changes in electrical resistance in ultra rapid annealing[43]. These only consider the crystallinity, and do not directly observe the grain size of α-Fe during annealing. The major scientific advance in this study is the quantitative discussion of kinetics based on time-resolved detection of both crystallinity and grain size from SXRD and further detailed investigation of the microstructure using TEM/APT.

To summarize the above findings and discussions, Fig. 4 shows a schematic of the microstructural evolution with isothermal temperature and elapsed time. There were three stages of crystallization: the precursor amorphous phase, Cu clustering, and finally the α-Fe nanocrystallization. These stages and the final microstructures strongly depended on both the temperature and time. However, the kinetics of α-Fe nanocrystallization process was unchanged against the isothermal temperature, which sporadically followed by the diffusion-controlled reactions. Therefore, it can be concluded that the Cu cluster size and distribution are the most important factors controlling the microstructure of the Fe-Si-B-P-Cu-C alloy. Because of the very low content of Cu and very short evolution time of Cu clustering, the experimental evaluation of Cu cluster kinetics is a very challenging task but important to fully understand the nanocrystallization kinetics of soft magnetic alloys.

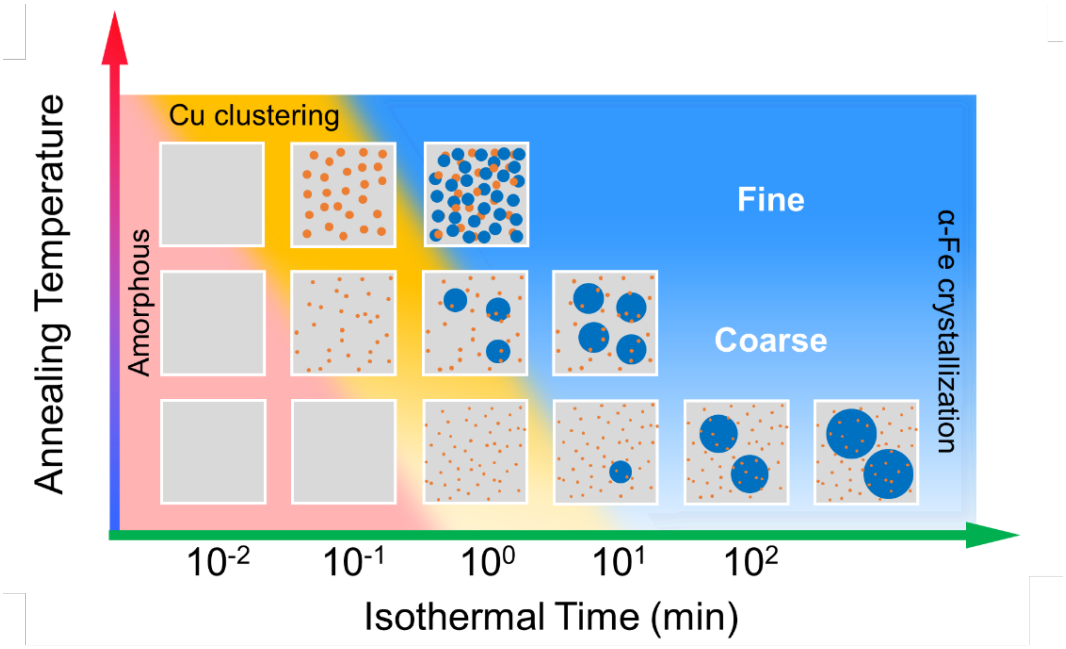


Figure. 4. Schematic of microstructure evolution with isothermal temperature and elapsed time. The square areas illustrate the microstructure consisting of amorphous (gray), Cu cluster (orange), and α-Fe grain (blue).

## Conclusions

In this study, the nanocrystallization mechanism of an Fe–Si–B–P–Cu–C alloy was investigated by means of multiprobe methods of TEM, APT, and *in situ* SRXD. Consequently, the nanocrystallization mechanism of this alloy was confirmed to be a sporadic nucleation process irrespective of the temperature. Although the nucleation process of α-Fe grains was unchanged against the temperature, the different Cu cluster size for different temperature significantly affected the growth rate and grain size of α-Fe nanocrystallization. For the higher temperature, the Cu cluster size became sufficiently large to function as nucleation site of α-Fe. Consequently, the microstructure of high-density fine grains of α-Fe was obtained during the short time of a few seconds. However, for the lower temperature, the Cu cluster size was excessively small to act as the nucleation sites of α-Fe, resulting in the low-density coarse grains of α-Fe with very long growth time of 100 min. Therefore, to obtain the optimal nanocrystalline microstructure for excellent soft magnetic properties, it is important to control the Cu clustering and subsequent α-Fe crystallization at higher temperature with shorter time.

## Acknowledgments

We thank Dr. S. Kawaguchi, Dr. S. Kobayashi, and Dr. Y. Mori for technical support with the SXRD measurements and Ms. K. Suzuki for TEM/APT sample preparation. The SPring-8 experiments were conducted with the approval of the Japan Synchrotron Radiation Research Institute (JASRI; Proposal Nos. 2022A1737, 2023A1793, and 2023B1747). This study was partially supported by the MEXT Program for the Creation of Innovative Core Technology for Power Electronics (Grant No. JPJ009777,

and the Data Creation and Utilization-Type Material Research and Development Project (Digital Transformation Initiative Center for Magnetic Materials) Grant No. JPMXP1122715503.

**Author Contributions**

Shozo Hiramoto: Conceptualization (lead), investigation (lead), methodology (lead), data curation (lead), formal analysis (lead), validation (lead), visualization (lead), writing the original draft (lead), writing the review, and editing (lead). Jun Uzuhashi: Investigation (supporting), methodology (supporting), visualization (supporting), writing–review and editing (supporting). Satoshi Okamoto: Project administration (equal); writing, review, and editing (supporting). Tadakatsu Ohkubo: Project administration (equal); writing-review and editing (supporting). Akihiko Toda: Formal analysis (supporting); validation (supporting); writing, review, and editing (supporting). Sangwook Kim: Writing, reviewing, and editing (Supporting Information). Chikako Moriyoshi: Conceptualization (supporting), investigation (supporting), methodology (supporting), writing–review, and editing (supporting). Yoshihiro Kuroiwa: Project administration (equal); conceptualization (supporting); Supervision; Writing, review, and editing (supporting).

**Declarations**

All authors declare no conflict of interest.

**Data availability**

Data supporting the findings of this study are available from the corresponding author upon request.

**References**

[1] Silveyra JM, Ferrara E, Huber DL, Monson TC (2018) Soft magnetic materials for a sustainable and electrified world. Science 362:eaao0195. doi: 10.1126/science.aao0195

[2] Herzer G (1990) Grain size dependence of coercivity and permeability in nanocrystalline ferromagnets. IEEE Trans Magn 26:1397–1402. doi: 10.1109/20.104389

[3] Yoshizawa Y, Oguma S, Yamauchi K (1988) New Fe-based soft magnetic alloys composed of ultrafine grain structure. J Appl Phys 64:6044–6046. doi: 10.1063/1.342149

[4] Hono K, Ping DH, Ohnuma M, Onodera H (1999) Cu clustering and Si partitioning in the early crystallization stage of an Fe73.5Si13.5B9Nb3Cu1 amorphous alloy. Acta Mater 47:997–1006. doi: 10.1016/S1359-6454(98)00392-9

[5] Pradeep KG, Herzer G, Choi P, Raabe D (2014) Atom probe tomography study of ultrahigh nanocrystallization rates in FeSiNbBCu soft magnetic amorphous alloys on rapid annealing. Acta Mater 68:295–309. doi: 10.1016/j.actamat.2014.01.031

[6] Köster U, Schünemann U, Blank-Bewersdorff M, Brauer S, Sutton M, Stephenson GB (1991) Nanocrystalline materials by crystallization of metal-metalloid glasses. Mater Sci Eng A

133:611–615. doi: 10.1016/0921-5093(91)90146-E

[7] Hermann H, Mattern N, Roth S, Uebele P (1997) Simulation of crystallization processes in amorphous iron-based alloys. Phys Rev B 56:13888–13897. doi: 10.1103/PhysRevB.56.13888

[8] Ohta M, Yoshizawa Y (2007) Magnetic properties of nanocrystalline Fe82.65Cu1.35SixB16−x alloys (x=-7). Appl Phys Lett 91 062517. doi: 10.1063/1.2769956

[9] Urata A, Matsumoto H, Yoshida S, Makino A (2011) Fe–Si–B–P–Cu nanocrystalline alloy ribbons with high saturation magnetic flux density prepared using industrial materials IEEE Trans Magn 47:3177–3179. doi: 10.1109/TMAG.2011.2158198

[10] Urata A, Matsumoto H, Yoshida S, Makino A (2011) Fe–B–P–Cu nanocrystalline soft magnetic alloys with high Bs. J Alloys Compd 509:S431–S433. doi: 10.1016/j.jallcom.2010.12.104

[11] Suzuki K, Parsons R, Zang B, Onodera K, Kishimoto H, Shoji T, Kato A (2018) Nano-crystallization of amorphous alloys by ultra-rapid annealing: An effective approach to magnetic softening. J Alloys Compd 735:613–618. doi: 10.1016/j.jallcom.2017.11.110

[12] Allia P, Barricco M, Knobel M, Tiberto P, Vinai F (1994) Soft nanocrystalline ferromagnetic alloys with improved ductility obtained through dc Joule heating of amorphous ribbons. J Magn Magn Mater 133:243–247. doi: 10.1016/0304-8853(94)90536-3

[13] Morsdorf L, Pradeep KG, Herzer G, Kovács A, Dunin-Borkowski RE, Povstugar I et al. (2016) Phase selection and nanocrystallization in Cu-free soft magnetic FeSiNbB amorphous alloy upon rapid annealing. J Appl Phys 119:124903. doi: 10.1063/1.4944595

[14] Zang B, Parsons R, Onodera K, Kishimoto H, Kato A, Liu ACY, Suzuki K (2017) Effect of heating rate during primary crystallization on soft magnetic properties of melt-spun Fe-B alloys. Scr Mater 132:68–72. doi: 10.1016/j.scriptamat.2017.01.030

[15] Wang Y, Zhang Y, Takeuchi A, Makino A, Kawazoe Y (2016) Investigation on the crystallization mechanism difference between FINEMET® and NANOMET® type Fe-based soft magnetic amorphous alloys. J Appl Phys 120:145102. doi: 10.1063/1.4964433

[16] Urata A, Yamaki M, Matsumoto H, Yoshida S, Makino A (2016) Alloy composition, Fe-based nanocrystalline alloy and its manufacturing method, and magnetic parts. JP Patent, P6046357.

[17] Nomura Y, Uzuhashi J, Tomita T, Takahashi T, Kuwata H, Abe T et al. (2021) Heating rate dependence of coercivity and microstructure of Fe–B–P–Cu nanocrystalline soft magnetic materials. J Alloys Compd 859:157832. doi: 10.1016/j.jallcom.2020.157832

[18] Takenaka K, Setyawan AD, Sharma P, Nishiyama N, Makino A (2016) Industrialization of nanocrystalline Fe–Si–B–P–Cu alloys for high magnetic flux density cores. J Magn Magn Mater 401:479–483. doi: 10.1016/j.jmmm.2015.10.091

[19] Zhang Z, Sharma P, Makino A (2012) Role of Si in high Bs and low core-loss Fe85.2B10−XP4Cu0.8SiX nano-crystalline alloys. J Appl Phys 112:103902. doi: 10.1063/1.4765718

[20] Matsuura M, Nishijima M, Takenaka K, Takeuchi A, Ofuchi H, Makino A (2015) Evolution of fcc Cu clusters and their structure changes in the soft magnetic Fe85.2Si1B9P4Cu0.8

(NANOMET) and FINEMET alloys observed by X-ray absorption fine structure. J Appl Phys 117:17A324. doi: 10.1063/1.4916937

[21] Sharma P, Zhang X, Zhang Y, Makino A (2015) Competition driven nanocrystallization in high Bs and low coreloss Fe–Si–B–P–Cu soft magnetic alloys. Scr Mater 95:3–6. doi: 10.1016/j.scriptamat.2014.08.023

[22] Kawaguchi S, Takemoto M, Osaka K, Nishibori E, Moriyoshi C, Kubota Y et al. (2017) High-throughput powder diffraction measurement system consisting of multiple MYTHEN detectors at beamline BL02B2 of SPring-8. Rev Sci Instrum 88:085111. doi: 10.1063/1.4999454

[23] Makino A, Kubota T, Yubuta K, Inoue A, Urata A, Matsumoto H, Yoshida S (2011) Low core losses and magnetic properties of Fe85-86Si1-2B8P4Cu1 nanocrystalline alloys with high B for power applications (invited). J Appl Phys 109:07A302. doi: 10.1063/1.3535169

[24] Scherrer P (1918) Determination of the size and internal structure of colloidal particles using X-rays. Nachr Ges Wiss Goettingen Math Phys 2:98–100.

[25] Borrego JM, Conde CF, Conde A, Grenèche JM (2001) Crystallization of Co-containing Finemet alloys. J Non-Crystal Solids 287:120–124. doi: 10.1016/S0022-3093(01)00544-0

[26] Uzuhashi J, Ohkubo T, Hono K (2023) Development of automated tip preparation for atom probe tomography by using script-controlled FIB-SEM. Ultramicroscopy 247:113704. doi: 10.1016/j.ultramic.2023.113704

[27] Uzuhashi J, Ohkubo T, Hono K (2024) An automated site-specific tip preparation method for atom probe tomography using script-controlled focused ion beam/scanning electron microscopy. Microsc Microanal 00:1–6. doi: 10.1093/mam/ozae015

[28] Kolmogorov AN (1937) On the Statistical Theory of Crystallization of Metals (in Russian). Bull Acad Sci USSR Math Ser 1:355–359.

[29] Johnson WA, Mehl RF (1939) Reaction kinetics in processes of nucleation and growth. Am Inst Min Metall Eng 135:416.

[30] Avrami M (1939) Kinetics of phase change. I General theory. J Chem Phy 7:1103–1112. doi: 10.1063/1.1750380

[31] Avrami M (1940) Kinetics of phase change. II Transformation-time relations for random distribution of nuclei, J Chem Phys 8:212–224. doi: 10.1063/1.1750631

[32] Avrami M (1941) Granulation, phase change, and microstructure kinetics of phase change. III. J Chem Phys 9:177–184. doi: 10.1063/1.1750872

[33] Aaron HB, Fainstein D, Kotler GR (1970) Diffusion-limited phase transformations: a comparison and critical evaluation of the mathematical approximations. J Appl Phys 41:4404–4410. doi: 10.1063/1.1658474

[34] Schawe JEK, Wrana C (2020) Competition between structural relaxation and crystallization in the glass transition range of random copolymers. Polymers 12:1778. doi: 10.3390/polym12081778

[35] Calef DF, Deutch JM (1983) Diffusion-controlled reactions. Ann Rev Phys Chem 34:493–524.

doi: 10.1146/annurev.pc.34.100183.002425

[36] Sanati M, Zunger A (2007) Evolution of L 12 ordered domains in fcc Cu3Au alloy. J Phys Condensed Mat 19:086201. doi: 10.1088/0953-8984/19/8/086201

[37] Hono K, Hiraga K, Wang Q, Inoue A, Sakurai T (1992) The microstructure evolution of a Fe73.5Si13.5B9Nb3Cu1 nanocrystalline soft magnetic material. Acta Metall Mater 40:2137–2147. doi: 10.1016/0956-7151(92)90131-W

[38] Zhang Y, Hono K, Inoue A, Sakurai T (1996) APFIM studies of nanocrystalline microstructural evolution in Fe-Zr-B(-Cu) amorphous alloys. Mater Sci Eng A 217–218:407–413. doi: 10.1016/S0921-5093(96)10285-9

[39] Ayers JD, Harris VG, Sprague JA, Elam WT, Jones HN (1998) On the formation of nanocrystals in the soft magnetic alloy Fe73.5Nb3Cu1Si13.5B9. Acta Mater 46:1861–1874. doi: 10.1016/S1359-6454(97)00436-9

[40] Ohnuma M, Hono K, Linderoth S, Pedersen JS, Yoshizawa Y, Onodera H (2000) Small-angle neutron scattering and differential scanning calorimetry studies on the copper clustering stage of Fe–Si–B–Nb–Cu nanocrystalline alloys. Acta Mater 48:4783–4790. doi: 10.1016/S1359-6454(00)00277-9

[41] Ohkubo T, Kai H, Ping DH, Hono K, Hirotsu Y (2001) Mechanism of heterogeneous nucleation of α-Fe nanocrystals from Fe89Zr7B3Cu1 amorphous alloy. Scr Mater 44:971–976. doi: 10.1016/S1359-6462(00)00689-8

[42] Miao XF, Wang YG (2012) Crystallization mechanism and its correlation with structural and soft magnetic properties of FeSiBPCu nanocrystalline alloys Journal of Materials Science 47: 1745-1750. doi: 10.1007/s10853-011-5954-1

[43] Zang B, Parsons R, Onodera K, Kishimoto H, Shoji T, Kato A et al. (2020) Nanostructural formation kinetics in an Fe86B14 soft magnetic alloy investigated by in situ transport measurements under isothermal conditions Physical Review Materials 4: 033404. doi: 10.1103/PhysRevMaterials.4.033404